The Meteoritical Society

Meteoritics & Planetary Science 46, Nr 1, 21–34 (2011)
doi: 10.1111/j.1945-5100.2010.01141.x

New insights into the mineralogy and weathering of the Meridiani Planum meteorite, Mars

Iris FLEISCHER[1*], Christian SCHRÖDER[2], Göstar KLINGELHÖFER[1], Jutta ZIPFEL[3], Richard V. MORRIS[4], James W. ASHLEY[5], Ralf GELLERT[6], Simon WEHRHEIM[1], and Sandro EBERT[1]

[1]Institut für Anorganische und Analytische Chemie, Johannes-Gutenberg-Universität Mainz, Staudinger Weg 9, 55128 Mainz, Germany
[2]Universität Bayreuth und Eberhard Karls Universität Tübingen, Sigwartstr. 10, 72076 Tübingen, Germany
[3]Senckenberg Forschungsinstitut und Naturmuseum Frankfurt, Sektion Meteoritenforschung, Senckenberganlage 25, 60325 Frankfurt, Germany
[4]ARES Code KR, NASA Johnson Space Center, 2101 NASA Parkway, Houston, Texas 77058, USA
[5]Mars Space Flight Facility, School of Earth and Space Exploration, Arizona State University P.O. Box 876305, Tempe, Arizona 85287–6305, USA
[6]Department of Physics, University of Guelph, 50 Stone Road East, Guelph, Ontario N1G 2W1, Canada
[*]Corresponding author. E-mail: fleischi@uni-mainz.de

(Received 18 November 2009; revision accepted 15 October 2010)

Abstract–Meridiani Planum is the first officially recognized meteorite find on the surface of Mars. It was discovered at and named after the landing site of the Mars Exploration Rover Opportunity. Based on its composition, it was classified as a IAB complex iron meteorite. Mössbauer spectra obtained by Opportunity are dominated by kamacite (α-Fe-Ni) and exhibit a small contribution of ferric oxide. Several small features in the spectra have been neglected to date. To shed more light on these features, five iron meteorite specimens were investigated as analogs to Meridiani Planum with a laboratory Mössbauer setup. Measurements were performed on (1) their metallic bulk, (2) troilite (FeS) inclusions, (3) cohenite ($(Fe,Ni,Co)_3C$) and schreibersite ($(Fe,Ni)_3P$), and (4) corroded rims. In addition to these room-temperature measurements, a specimen from the Mundrabilla IAB-ungrouped meteorite was measured at Mars-equivalent temperatures. Based on these measurements, the features in Meridiani Planum spectra can be explained with the presence of small amounts of schreibersite and/or cohenite and iron oxides. The iron oxides can be attributed to a previously reported coating on Meridiani Planum. Their presence indicates weathering through the interaction of the meteorite with small amounts of water.

INTRODUCTION

In January 2005, almost 1 year after landing at Meridiani Planum, the Mars Exploration Rover (MER) Opportunity investigated the heat shield that had been dropped during the entry, descent, and landing (EDL) sequence. Just a few meters from the heat shield, an intriguing rock with a pitted surface and a maximum dimension of approximately 30 cm was discovered and informally named "Heat Shield Rock" (Schröder et al. 2008). Though additional meteorites have been identified on Mars since this early find (e.g., Schröder et al. 2008; Ashley et al. Forthcoming), this rock is the only one currently recognized by the Meteoritical Society Committee on Meteorite Nomenclature, and was officially named Meridiani Planum after the location of its find (Connolly et al. 2006).

The chemical composition of Meridiani Planum derived from alpha particle X-ray spectrometer (APXS) data is 93% Fe, 7% Ni, approximately 300 ppm Ge and <100 ppm Ga (R. Gellert, personal communication). Based on Ni, Ge, and Ga contents,

Meridiani Planum was classified as a IAB complex iron meteorite (Connolly et al. 2006).

Meridiani Planum Mössbauer spectra were obtained on the undisturbed as well as on the brushed surface of the meteorite. They show kamacite as the dominant phase, together with small amounts of ferric oxide. False-color panoramic camera (Pancam) images revealed patches of an intriguing coating that appear more purple compared to the majority of the surface, as shown in Fig. 1. Schröder et al. (2008) described the coating in detail, but could not determine whether it represents remnants of a fusion crust or whether it is a product of chemical weathering.

Here we show the results of a more detailed analysis of the Mössbauer spectra obtained of Meridiani Planum. Several minor features in the spectra had not been explained previously (e.g., Van Cromphaut et al. 2007). We try to interpret these spectra by comparing them to Mössbauer spectra of analog iron meteorites taken in the laboratory under Mars-equivalent conditions. In addition, we analyzed the 6.4 keV spectra obtained with Opportunity's Mössbauer instrument. Only 14.4 keV spectra were analyzed previously. Comparing the 6.4 keV and 14.4 keV Mössbauer spectra yields depth-selective information because of the energy-dependent attenuation in the investigated targets (see the Depth Selective Information Extracted from Mössbauer Spectra section for details). This approach shows the presence of previously unidentified mineral phases, and supports a weathering rind (not a fusion crust) interpretation for the coating.

METHODS

Mars Exploration Rover Scientific Payload

The two MER Spirit and Opportunity are equipped with both mast-mounted remote sensing instruments and contact instruments mounted on a 5-degree-of-freedom instrument deployment device (IDD; Squyres et al. 2003). The remote sensing instruments include a multiple filter visible to near-infrared (400 to 1010 nm) panoramic camera (Pancam) (Bell et al. 2003) and a miniature thermal emission spectrometer (Mini-TES) covering the wavelength region from 5–29 μm (Christensen et al. 2003). The contact instruments comprise a rock abrasion tool (RAT) to remove surface contamination or coatings by brushing or grinding into a rock (Gorevan et al. 2003), a 30 μm per pixel microscopic imager (MI) (Herkenhoff et al. 2003), an APXS for chemical analysis (Rieder et al. 2003), and a miniaturized Mössbauer spectrometer (MIMOS II) to determine the iron mineralogy (Klingelhöfer et al. 2003).

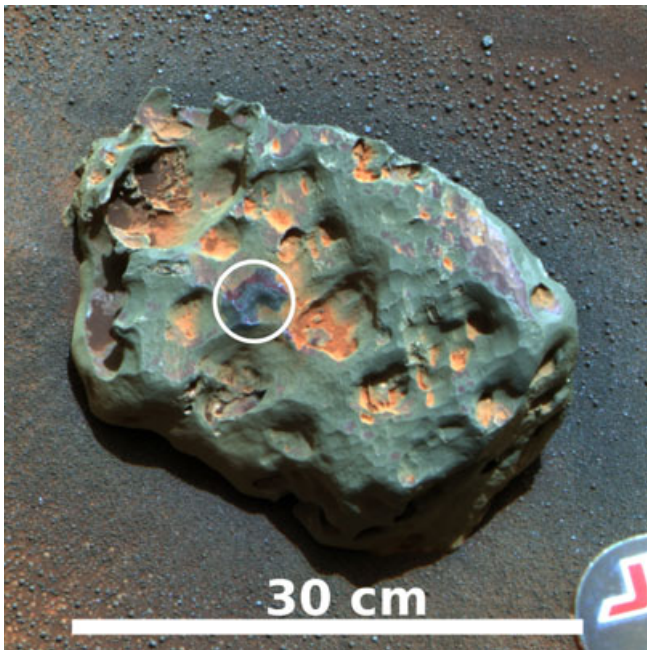

Fig. 1. False color Pancam image (filters L2, L5, and L7) obtained on Meridiani Planum. The brushed area is marked with a circle. The meteorite surface shows pits and is partially coated with a material that appears purple (http://marswatch.astro.cornell.edu/pancam_instrument/images/False/Sol352B_P2596_1_False_L257.jpg).

Mössbauer Data Analysis and Instrumentation

Numerous publications provide extensive reviews of Mössbauer spectroscopy (e.g., Wegener 1966; Gonser 1975; Gütlich et al. 1978; Hawthorne 1988) and its applications in mineralogy and geochemistry (e.g., Bancroft 1973; Hawthorne 1988; Mitra 1992; Burns 1993; McCammon 1995; Murad and Cashion 2004; Dyar et al. 2006). Briefly, the Mössbauer effect is the recoilless absorption and emission of γ-rays by nuclei of certain isotopes bound in a solid. A Mössbauer experiment consists of a radioactive source (^{57}Co for Mössbauer spectroscopy with ^{57}Fe), an absorber, and a detector. Generally, the source and absorber will be different compounds. As the chemical environment influences nuclear energy levels, resonance lines will be shifted against each other. This shift can be compensated for by moving the source relative to the sample, using the Doppler effect to shift the energy of emitted γ-rays. The positions of resonance lines are usually referred to by their Doppler velocity. A typical velocity range for Mössbauer spectroscopy with ^{57}Fe is on the order of ± 10 mm s^{-1}, corresponding to an energy shift of approximately 10^{-8} eV in the case of the 14.4 keV γ-rays emitted from the ^{57}Co source.

Electric and magnetic interactions of ^{57}Fe nuclei with their environment manifest themselves as

observable parameters in Mössbauer spectra: the center shift δ, the quadrupole splitting ΔE_Q, and the hyperfine magnetic field B_{hf}. Based on these parameters, a large number of iron bearing compounds can be distinguished and properties such as the oxidation states of iron can be determined.

The center shift δ is the shift of the centroid of a (sub)spectrum against a zero reference point of the Doppler velocity, measured relative to a reference absorber (α-iron in this work). The center shift is comprised of the temperature-independent isomer shift and the temperature dependent second-order Doppler shift. The isomer shift results from Coulomb interaction of the positive nuclear charge distribution and the electron charge density at the nucleus. The second order Doppler shift is a small thermal shift due to lattice vibrations that can only be observed if source and sample are at different temperatures (e.g., Murad and Cashion 2004), a situation that typically arises for laboratory setups where the sample is mounted inside a cryostat and the source is kept at room temperature. For the MER MIMOS II instruments, the investigated sample, the instrument, and the internal reference target are always at approximately the same temperature, with a temperature offset of 10 K or less, and thus the temperature dependence of δ is negligible.

The quadrupole splitting ΔE_Q results from electric quadrupole interaction between the nuclear quadrupole moment and an electric field gradient. A nuclear quadrupole moment exists when the nucleus has a nonspherical shape, and an electric field gradient is typically present for local lattice symmetries other than cubic. In Mössbauer spectra, ΔE_Q manifests itself as a line pair ("doublet"). The separation between both line centers is equal to ΔE_Q.

Below the magnetic ordering temperature of paramagnetic substances a net magnetic hyperfine field B_{hf} is present at the nucleus. It interacts with the magnetic dipole moment of the nucleus and a six-line pattern ("sextet") is observed in Mössbauer spectra. The hyperfine field B_{hf} is proportional to the separation of the two outermost lines. If an additional electric quadrupole distortion is present, ΔE_Q can be extracted from the positions of lines (L) in the spectrum, numbered from left to right, as $\Delta E_Q = 1/2[(L6 - L5) - (L2 - L1)]$. The hyperfine field B_{hf} does and ΔE_Q can vary with temperature (e.g., because of magnetic or crystallographic transitions). For nanosized particles, generally < 30 nm, magnetic splitting may not be observed until a temperature well below the nominal magnetic ordering temperature is reached. This effect is called superparamagnetism.

The analysis of a Mössbauer spectrum yields subspectral areas of the different mineral phases contributing to the total spectrum, which are integrated and background-corrected areas under all peaks of a doublet or sextet phase. Deriving quantifications by weight from subspectral areas can be done, but requires the knowledge of correction factors for all identified phases, which are not easily available (i.e., Debye-Waller factors; e.g., Wegener 1966; Gütlich et al. 1978; Mössbauer 2000; Murad and Cashion 2004). Here, we do not calculate weight percentages, but report subspectral areas as a means of quantification of phase abundances.

According to basic principles, resonance lines in Mössbauer spectra exhibit a Lorentzian shape. Lines may broaden and deviate from a purely Lorentzian shape through the influence of various effects. The "cosine-smearing effect" is related to the geometry of the experimental setup. This effect leads to broadened lines with asymmetric shapes and shifts line centers outwards, particularly at higher velocities (e.g., Riesenman 1969; Aramu and Maxia 1970). It must be noted, however, that the source radiation in MIMOS II is collimated so as to minimize geometrical effects of the experimental setup, for example, to keep the outer lines of hematite and maghemite distinguishable in a spectrum. If a Mössbauer line passes through a resonantly absorbing sample, γ-rays from the center of the line (i.e., at maximum resonance) are absorbed preferably. In a thick sample, the central part of the line is thus reduced in intensity and as a result of this thickness effect, the line broadens (e.g., Margulies and Ehrmann 1961; Fultz and Morris 1981).

The MER MIMOS II instruments measure spectra of soil and rock targets in backscattering geometry with the primary ^{57}Co source. Spectra are stored in 13 separate temperature windows 10 K wide between 180 K and 290 K, as well as below 180 K and above 290 K (Klingelhöfer et al. 2003). Calibration is carried out with a secondary source and an internal absorber in transmission geometry. The MER calibration absorber is composed of α-iron, hematite, and magnetite.

The elemental composition of investigated targets is important context information for the analysis of Mössbauer spectra. This information is provided through measurements made with the APXS (Rieder et al. 2003; Brückner et al. 2008).

All laboratory measurements were carried out with a MIMOS II instrument equivalent to the spectrometer on board the Opportunity rover. Low-temperature measurements were performed in a climate chamber cooled with liquid nitrogen. Both the MIMOS II sensorhead and the sample were mounted inside the chamber. Measurements were performed under a dry nitrogen atmosphere at approximately 10 mbar pressure. For laboratory measurements, calibration measurements were carried out with a metallic α-iron foil.

Depth Selective Information Extracted from Mössbauer Spectra

Iron-nickel meteorites may exhibit a fusion crust or a weathered layer that formed after their impact. Depth selective Mössbauer spectroscopy may provide information about the distribution of iron-bearing phases in such a surface layer and the underlying bulk rock. The MER MIMOS II instruments detect both the resonant 14.4 keV γ-rays and the resonant 6.4 keV X-rays simultaneously (Klingelhöfer et al. 2003; Fleischer et al. 2008a). Because of their higher energy, 14.4 keV γ-rays have a greater penetration (or escape) depth than 6.4 keV X-rays. The thickness and composition of a surface layer can be estimated by simulating and comparing 6.4 keV and 14.4 keV Mössbauer spectra, as described in detail by Fleischer et al. (2008a). This simulation models the backscattered spectra based on the composition of the surface layer and bulk of the sample, respectively, taking into account the energy dependent absorption coefficients of 6.4 keV and 14.4 keV radiation. The effect of the surface layer on the spectra will be largest if a significant portion of the 14.4 keV radiation reaches the detectors from the bulk of the sample, while most of the detected 6.4 keV radiation stems from within the surface layer (see Fleischer et al. 2008a for further explanations). Typical maximum sampling depths (i.e., the thickness of the surface layer that allows the detection of a substrate at the detection limit of approximately 2%) are approximately 530 μm for 14.4 keV radiation and approximately 130 μm for 6.4 keV radiation, respectively, in basaltic rock, and approximately 50 μm for both energies in metallic iron (Fleischer et al. 2008b). Reconciling depth selective Mössbauer data with elemental data from the APXS would be straightforward if both instruments were analyzing the same material. However, the two instruments have different fields of view (approximately 15 mm diameter for the Mössbauer instrument, approximately 38 mm for the APXS) and the APXS sampling depth is considerably smaller (approximately 1–20 μm; Gellert et al. 2006) than that of the Mössbauer instrument.

Analysis of the Meridiani Planum Meteorite and Analog Specimens

All measurements with contact instruments were made on the surface of the Meridiani Planum meteorite that may have been heat-affected during the fall of the meteorite through the Martian atmosphere and later exposed to physical and chemical weathering on the Martian surface. Mössbauer spectra of the meteorite were obtained on the undisturbed and on the brushed surface in 10 K-wide temperature windows in the temperature range between 200 K and 270 K. Because of mission time constraints, the integration time for a given temperature window is limited, so that counting statistics are not optimal compared to laboratory spectra where virtually unlimited integration times may be available. To compensate for low counting statistics in individual temperature windows, spectra have often been summed over a larger temperature range in the course of the MER mission (e.g., Morris et al. 2006a, 2006b, 2008). Mössbauer spectra obtained on Meridiani Planum have been interpreted as a mixture of kamacite and a minor ferric phase characterized by a doublet attributed to "nanophase ferric oxide" (npOx; iron oxides or oxyhydroxides with particle sizes in the nanometer range that are superparamagnetic at the temperature of observation, including hematite (α-Fe_2O_3), goethite (α-FeOOH), akaganéite (β–FeO(OH, Cl)) or lepidocrocite (γ-FeOOH)) (Morris et al. 2006a).

In this study, we present a temperature-dependent analysis that also takes into account a number of minor spectral features, indicating the presence of at least one additional iron-bearing mineral phase. Although the spectral features are just above the limit of background counts, they appear consistently in many single temperature window spectra and thus deserve further consideration. The spectral features are visible most clearly in the sum of all spectra (14.4 keV plus 6.4 keV) obtained on the brushed meteorite surface. Due to their low intensity, a fit only yields satisfactory results if constraints for Mössbauer parameters are implemented in the fit model. This requires the knowledge of Mössbauer parameters of candidate mineral phases.

Five iron meteorite specimens with compositions similar to Meridiani Planum were investigated as analogs. Their classification and Ni, Ge, and Ga contents are summarized in Table 1. The analog specimens are shown in Fig. 2. Three of them, from Mundrabilla (Fig. 2a), Canyon Diablo (Fig. 2b), and Bear Creek (Fig. 2c) have a metallic matrix with approximately centimeter-sized inclusions of troilite (FeS), schreibersite ($(Fe,Ni)_3P$), and cohenite ($(Fe,Ni,Co)_3C$). The Canyon Diablo and Bear Creek specimens had been etched prior to this study and exhibit a well-defined Widmanstätten pattern. The two specimens from North Chile (Fig. 2d) and Shişr 043 (Fig. 2e) are practically free from inclusions. The Canyon Diablo, Bear Creek, and Shişr 043 specimens exhibit corroded rims that were investigated for comparison with the surface coating of Meridiani Planum. The Mundrabilla specimen was investigated at Mars-equivalent temperatures (190 K to 300 K); all other specimens were measured at room temperature.

Table 1. Classification and Ni, Ge, and Ga contents of analog iron meteorites.

Meteorite	Classification	Composition			Reference
		Ni (wt%)	Ga (ppm)	Ge (ppm)	
Mundrabilla	IAB-ungrouped	7.9	67	173	Weinke 1977
Canyon Diablo	IAB octahedrite	6.8–7[a]	78–85[a]	280–360[a]	Wasson and Ouyang 1990
Bear Creek	IIIAB octahedrite	10.14	15	25	Lovering et al. 1957
North Chile	IIAB hexahedrite	5.27–5.65	57–62	170–190	Wasson and Goldstein 1968
Shişr 043	IIIAB octahedrite	8.1	18.8	36.2	Al-Kathiri et al. 2006

[a]Based on analyses of 15 specimens; Wasson and Ouyang 1990.

For the analysis of Mössbauer spectra, contributions from kamacite, troilite, and cohenite were modeled with one sextet each. Schreibersite has three crystallographic sites for metal atoms, and schreibersite spectra have been described with three sextets corresponding to these crystallographic sites (Bailey and Duncan 1967; Ouseph et al. 1979). Although a detailed study of the magnetic structure of Fe_3P (Lisher et al. 1974) revealed that the spectra can be fitted with up to six sextets (two for each site), we were able to satisfactorily fit schreibersite from the Mundrabilla specimen with three sextets.

Fits of the sum of all Mössbauer spectra (14.4 keV and 6.4 keV) obtained on the brushed surface of Meridiani Planum are shown in Fig. 3. Mössbauer hyperfine parameters and subspectral areas are listed in Tables 2 and 3, respectively. Representative spectra obtained on analog specimens are shown in Fig. 4, representative Mössbauer parameters from analog measurements and from other studies are listed in Table 4. Temperature dependent Mössbauer parameters for kamacite from Mundrabilla are listed in Table 5.

RESULTS AND DISCUSSION

Kamacite and Taenite in Meridiani Planum

The metallic matrix of iron meteorites is composed of iron-nickel compounds, described in detail by Mittlefehldt et al. (1998): Kamacite, body-centered cubic α-Fe-Ni, has Ni contents <6 wt% and forms extensive lamellae upon cooling in a Widmanstätten pattern. Areas with higher Ni contents are often generally referred to as taenite, although they may be complex in composition. Within a few micrometers of the kamacite interphase, the Ni contents of taenite lamellae rise to approximately 50% and drop to lower contents at the center of the lamellae. The phase with 50% Ni exhibits tetragonal ordering (“tetrataenite”). Areas with Ni contents between 30% and 50% are intergrowths of tetrataenite and a body-centered cubic phase referred to as α_2-Fe-Ni. A submicron intergrowth of Ni-rich and Ni-poor phases is termed “plessite.” Kamacite and ordered taenite are each characterized by a sextet in Mössbauer spectra. A paramagnetic taenite phase, characterized by a singlet, may also be observed (e.g., Rancourt and Scorzelli 1995; Rancourt et al. 1999).

Mössbauer spectra of the Meridiani Planum meteorite are dominated by a magnetically ordered phase, which can be modeled with a single sextet attributed to kamacite. A single sextet, however, does not represent the spectral line shapes very well, which may be a consequence of line broadening due to geometry- and/or thickness-effects (cf. the Mössbauer Data Analysis and Instrumentation section) or due to the presence of taenite. As shown in Table 4, Mössbauer parameters very similar to those of the kamacite sextet have been reported for magnetically ordered taenite (cf. De Grave et al. 1992; Abdu and Ericsson 1997; Dunlap 1997; Ortalli and Pedrazzi 1990; Wojnarowska et al. 2008). In all these studies, B_{hf} of taenite was found to be slightly smaller than B_{hf} of kamacite. For the analog meteorite specimens, bulk Ni contents range from approximately 5.5% in North Chile (Wasson and Goldstein 1968) to approximately 10% in Bear Creek (Lovering et al. 1957). Based on these numbers, the presence of both kamacite and taenite is strongly expected in the Meridiani Planum meteorite and analog specimens, e.g., based on the Fe-Ni phase diagram (e.g., Reisener and Goldstein 2003). Taenite contents have been reported to be rather low for Canyon Diablo (up to 3 vol%; Vdovykin 1973) and comparably high for Mundrabilla (15–20% by area; Buchwald 1975). Clear evidence for the presence of taenite in a meteorite is the presence of a Widmanstätten pattern on the etched surfaces, as shown here for Canyon Diablo (Fig. 2b) and Bear Creek (Fig. 2c). Thirteen spots were measured on the metallic parts of analog specimens; three spots each on Canyon Diablo, Bear Creek, and Mundrabilla, and two spots each on North Chile and Shişr 043. To investigate whether thickness effects (see the Depth Selective Information Extracted from Mössbauer Spectra section) rather than admixture of taenite are responsible for the observed line-broadening, a stack of metallic α-iron foils with a total thickness of 200 μm was also measured with two different MIMOS II sensor heads: α-iron

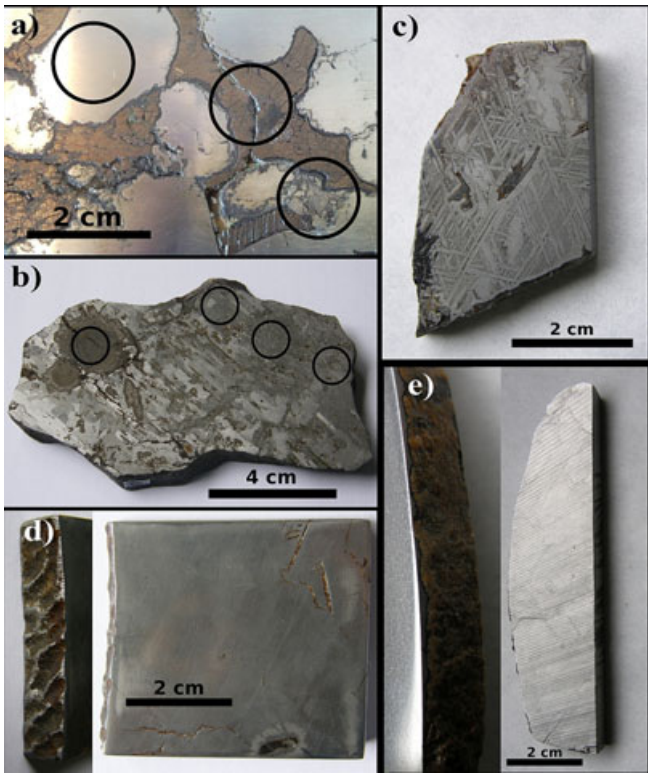

Fig. 2. Iron meteorite specimens measured as analogs for Meridiani Planum. a) Mundrabilla (not etched) with troilite and schreibersite inclusions. b) Canyon Diablo with larger troilite and numerous smaller inclusions, mainly troilite and cohenite. c) Bear Creek with a clear Widmannstätten pattern and some inclusions. d) North Chile, the inset (left) shows the corroded rim. e) Shişr 043 with a part of the rim covered by a weathering rind (inset). Where applicable, circles representative for the instrument field of view (approximately 1.5 cm) are indicated.

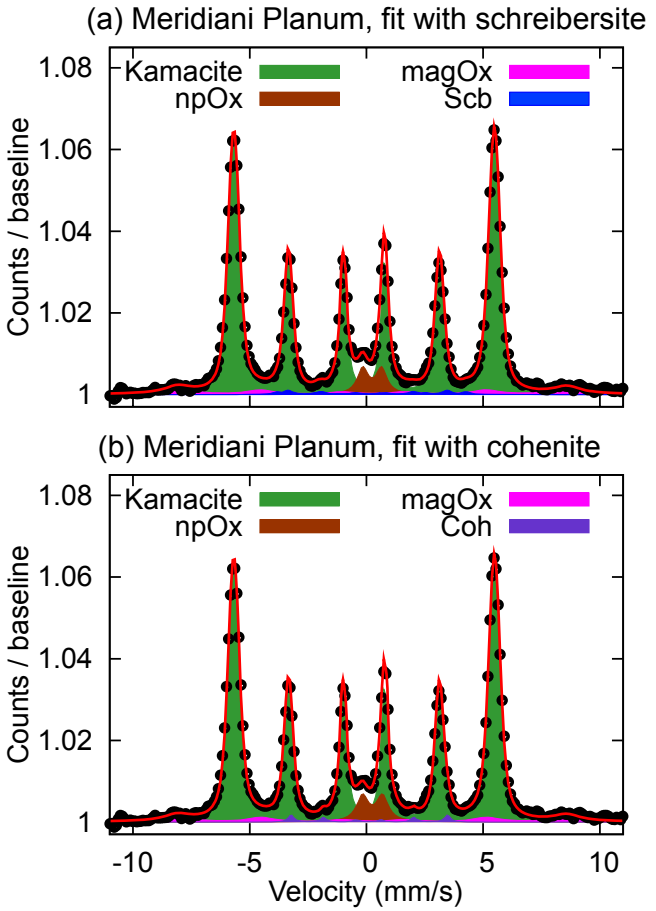

Fig. 3. Sum of 14.4 keV and 6.4 keV spectra obtained on the brushed surface of Meridiani Planum. npOx, nanophase ferric oxide; magOx, magnetically ordered iron oxides. a) Fit with schreibersite (Scb). b) Fit with cohenite (Coh). Due to the small amount of schreibersite/cohenite, their influence on the fit is small. Please refer to the online version of this article for color version of this figure.

provides a spectrum with B_{hf} in the same range as for kamacite and taenite (i.e., resonance lines are affected by broadening in a similar manner) and the certainty that only one phase is present.

Separate sextets corresponding to kamacite and taenite cannot be directly resolved, neither in spectra from the Meridiani Planum iron meteorite nor from analog specimens. To investigate possible line broadening due to the presence of taenite, line widths were evaluated pairwise for these spectra. Lines 1 and 6, lines 2 and 5, and lines 3 and 4 were set to have equal widths and heights in the fits. The width ratio of the outer two line pairs only (lines 1 and 6 versus lines 2 and 5) was calculated, because the innermost line pair (lines 3 and 4) of the sextet pattern is overlapping with the npOx doublet and/or other phases, which increases the uncertainty of determining line widths. Line widths and line width ratios are listed in Table 6. Line width ratios cover the range of values from 1.21 to 1.36. With values of 1.21 and 1.22, the two measurements on iron foils have the smallest line width ratios. With one exception for Bear Creek, all meteorite line width ratios are larger than 1.25. If taenite has a noteworthy influence on line broadening, large line width ratios would be expected for those meteorites with considerable taenite or plessite contents (e.g., Mundrabilla; Buchwald 1975), while the effect would be expected to be less pronounced for meteorites with low taenite or plessite contents (e.g., Canyon Diablo; Vdovykin 1973). However, the width ratios for both meteorites are in a similar range and even slightly larger for Canyon Diablo. The larger line width ratios observed for meteorite spectra may be an indication that line broadening is not only related to geometry and thickness effects and likely reflects the more complex metallographic structure compared to the iron foil, but the presence of magnetically ordered taenite in addition

Table 2. Temperature dependent Mössbauer hyperfine parameters for kamacite, nanophase ferric oxide (npOx), and magnetically ordered iron oxides (magOx) from Meridiani Planum.

		δ	ΔE_Q (mm s^{-1})	Γ	B_{hf} (T)	δ	ΔE_Q (mm s^{-1})	Γ	B_{hf} (T)
Mineral phase	T (K)	Undisturbed surface				Brushed surface			
Kamacite	205	0.00	0.00	0.29	35.2	−0.01	0.00	0.35	35.2
	215	0.00	0.00	0.31	35.0	0.00	0.00	0.35	35.0
	225	0.00	0.00	0.33	34.9	0.00	0.00	0.35	34.8
	235	0.01	0.00	0.34	34.7	0.00	−0.01	0.34	34.7
	245	0.02	0.00	0.32	34.5	0.02	0.00	0.29	34.5
	255	0.02	0.00	0.33	34.3	0.03	0.00	0.33	34.3
	265	0.02	0.00	0.33	34.2	0.03	0.00	0.37	34.2
Average values									
npOx	200–270	0.40	0.81		–	0.40	0.81		
magOx	200–270	0.39	−0.16		51.7	0.39	−0.16		51.7

Values of δ are given relative to metallic iron foil at the same temperature as the sample. Parameter uncertainties are ±0.02 mm s^{-1} for δ and ΔE_Q and ±0.2 T for B_{hf}.

Table 3. Subspectral areas for 6.4 keV and 14.4 keV spectra obtained on the undisturbed and brushed surface of Meridiani Planum.

		Subspectral area (%)		
	Mineral phase	14.4 keV	6.4 keV	6.4 keV + 14.4 keV
Undisturbed surface	Kamacite	90	88	
	npOx	5	5	
	Schreibersite/cohenite	2	2	
	magOx	3	5	
Brushed surface	Kamacite	84	84	86
	npOx	6	5	5
	Schreibersite/cohenite	3	4	3
	magOx	7	7	6

The uncertainties of subspectral areas are ±2% (absolute subspectral area).
For schreibersite/cohenite, Mössbauer parameters were constrained to values obtained from analog specimens. For all other phases, Mössbauer parameters were constrained to values obtained from summed Meridiani Planum spectra measured on the brushed surface. The sum of spectra obtained on the undisturbed surface was not fitted.

to kamacite cannot be inferred from line broadening. Paramagnetic taenite, characterized by a singlet (Table 4; Fig. 4), was not detected in spectra of Meridiani Planum either because (1) it strongly overlaps with the npOx-doublet, (2) the statistical quality of the spectra does not allow resolution of a singlet, or (3) this phase is not present in the meteorite in detectable amounts.

For Meridiani Planum, the good statistical quality of spectra from single temperature windows allows an extrapolation of low-temperature kamacite B_{hf} values to room temperature (Table 5; Fig. 5) for a direct comparison to values from analog samples. The extrapolation yields 33.7 T for the undisturbed as well as for the brushed surface, in good agreement with values from analog measurements or other studies, as reported in Table 4.

Laboratory measurements on meteorites are often carried out on polished meteorite slabs. On Meridiani Planum, however, the exposed surfaces that were measured had been affected by heating during the fall through the Martian atmosphere, followed by cooling and exposure to Martian weathering processes on the surface (further discussed in the following sections). The fall of a meteorite through Earth's atmosphere may lead to the formation of a fusion crust (e.g., El Goresy and Fechtig 1967) or surface layer through ablation and melting (e.g., Maringer 1960). Buchwald (1977) describes the occurrence of metastable α_2-iron with a hatched kamacite structure in the heat-affected surface zone of uncorroded iron meteorites. This zone may affect the outer 2–4 mm of the meteorite surface (Al-Kathiri et al. 2006). The effect of the Martian atmosphere may be less significant, but the thickness of the heat-affected surface layer may well be in the range of the sampling depth of the Mössbauer radiation (approximately 50 μm). The existence of a heat-affected surface layer possibly provides a further explanation for differences between Mössbauer parameters from Meridiani iron meteorites and analog samples, such as the slightly higher values for B_{hf} for Meridiani Planum compared to Mundrabilla (Fig. 5).

Identification of Schreibersite/Cohenite and Iron Oxides in Meridiani Planum

In addition to kamacite and npOx, Meridiani Planum spectra show minor, so far unexplained spectral

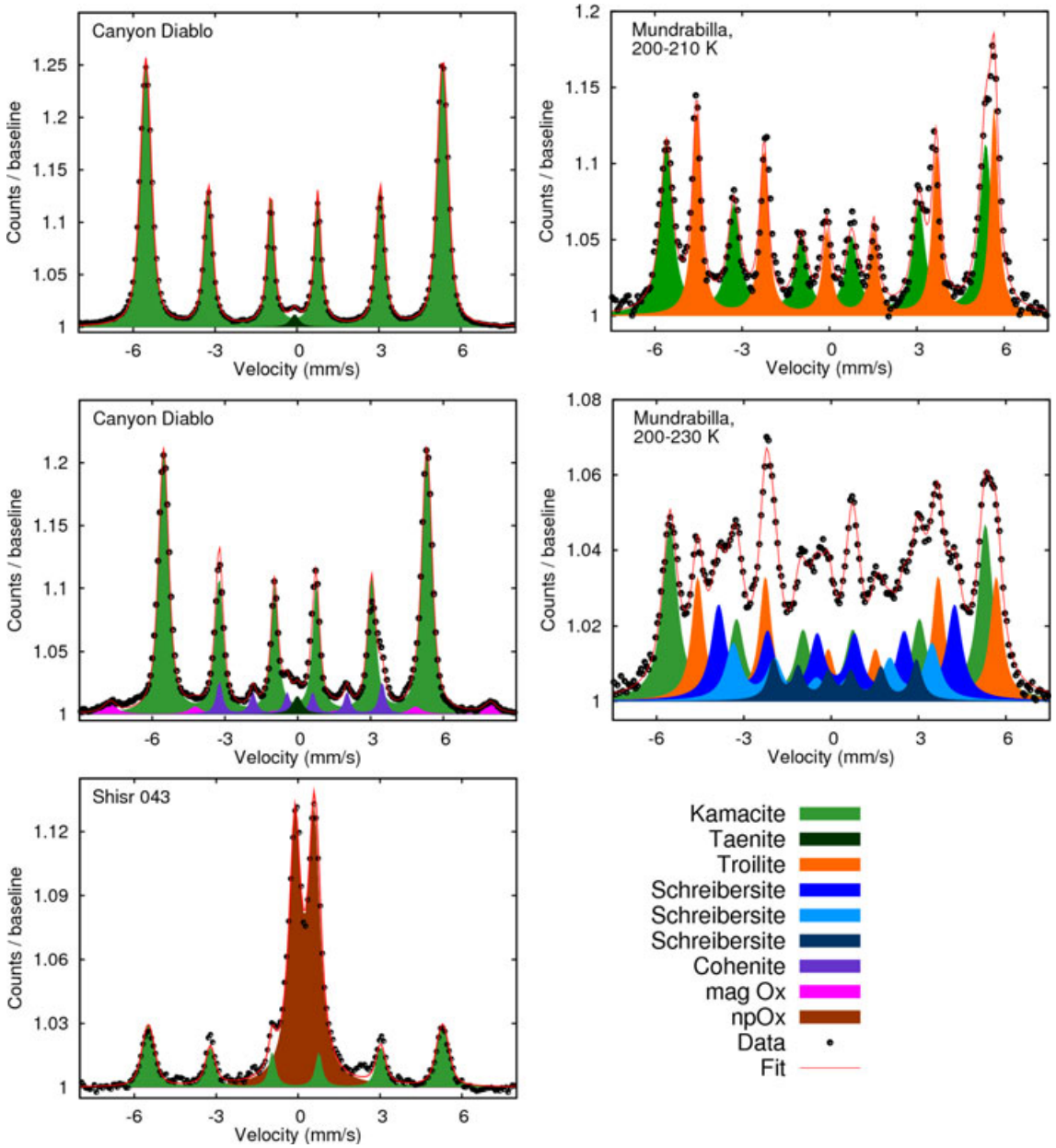

Fig. 4. Example spectra obtained on analog meteorite specimens. Troilite, cohenite and schreibersite inclusions did not fill the instrument field of view completely (cf. Fig. 2), leading to contributions of kamacite and/or troilite in the spectra. The spectra of Canyon Diablo and Mundrabilla were obtained on the polished surface (Figs. 2a and 2b); the spectrum of Shişr 043 was measured on the corroded surface rim (Fig. 2e). Please refer to the online version of this article for color version of this figure.

features. These are most apparent in the sum of all spectra (14.4 keV and 6.4 keV) obtained on the brushed meteorite surface. Separate fits were obtained from this sum as well as from the sums of 6.4 keV spectra obtained on the undisturbed and brushed surface, respectively, and from the sums of 14.4 keV spectra obtained on the undisturbed and brushed surface, respectively. The most pronounced of these features occur at approximately -8 mm s^{-1} and $+8.5$ mm s^{-1}, pointing to one or more sextets with rather large B_{hf}-values characteristic for iron oxides. A fit yields a sextet with broad lines, likely representing a composite of several overlapping sextets with similar parameters which arise from different iron oxides such as hematite (α-Fe_2O_3), maghemite (γ-Fe_2O_3), and potentially magnetite (Fe_3O_4). The sextet and the attributed phases will be referred to as "magOx." The parameters of the sextet were derived from the sum of all spectra

Table 4. Representative Mössbauer parameters from analog measurements and other studies (relative to α-iron; measured at room temperature unless indicated otherwise).

Phase	δ	ΔE_Q (mm s^{-1})	B_{hf} (T)	Meteorite	Reference
Chalcopyrite $CuFeS_2$	~ 0.30	~ 0.08	~ 35		Stevens et al. 2002
Chromite $FeCr_2O_4$	2 or 3 doublets; range of parameters				Stevens et al. 2002
Cohenite $(Fe, Ni, Co)_3C$	0.20	0.65	21.0		Wojnarowska et al. 2008
	0.20	0	20.9		Ouseph et al. 1979
	0.22	0.03	20.7	Canyon Diablo	This work
Daubreelite $FeCr_2S_4$	0.71	0.14	19.4		Stevens et al. 2002
Kamacite	0.08	−0.05	33.1	Torino	Ortalli and Pedrazzi 1990
	0.02	0	33.6	New Halfa	Abdu and Ericsson 1997
	0.01	0.02	33.4	Abee (Enstatite)	Dunlap 1997
	0.02	0	33.6	Morasko	Wojnarowska et al. 2008
	0.01	0	33.6	Canyon Diablo	This study
	0.02	0	34.4	Bear Creek	
	0.02	0	33.4	Shişr 043	
Mackinawite $(Fe, Ni)S_{0.9}$	0.91	0.09	29.8		Stevens et al. 2002
	0.85	0.06	26.2		
	0.88	0.09	22.8		
Pentlandite $(Fe, Ni)_9S_8$	~0.35	~0.35	–		Stevens et al. 2002
	~0.6	–	–		
magOx	0.32	−0.2	48.6	Canyon Diablo	This study
	0.34	−0.1	49.7	Bear Creek	
npOx	0.35	0.70	–	Shişr 043	This study
	0.34	0.77	–	Bear Creek	
Schreibersite $(Fe, Ni)_3P$	0.3	0.31	24.1	Mundrabilla (205 K)	This study
	0.26	0	21.2		
	0.45	0.31	16.2		
Pyrrhotite $Fe_{1-x}S$	~0.7	~0.15	~30		Stevens et al. 2002
	~0.7	~0.15	~28		
	~0.7	~0.15	~25		
Taenite (paramagnetic)	−0.02	0	–	Santa Catharina (180 K)	De Grave et al. 1992
	−0.10	0	–	Santa Catharina (300 K)	
	−0.08	0	–	Morasko	Wojnarowska et al. 2008
	−0.17	0	–	Morasko	
	0.10	0	–	Canyon Diablo	This study
	0	0	–	Canyon Diablo	
Taenite	−0.05	0.09	32.8	Torino	Ortalli and Pedrazzi 1990
(magnetically ordered)	0.12	0.12	30.3	New Halfa	Abdu and Ericsson 1997
	0.01	0.02	31.1	Abee (enstatite)	Dunlap 1997
	0	0	31.0	Morasko	Wojnarowska et al. 2008
Troilite FeS	0.74	−0.16	30.9	Mundrabilla (205 K)	This study
	0.75	−0.16	31.7	Mundrabilla (295 K)	

Values of δ are given relative to α-iron.
Uncertainties for this study are ±0.02 mm s^{-1} for δ and ΔE_Q and ±0.2 T for B_{hf}.

measured on the brushed surface and constrained to these values for all other fits (Table 2). As shown in Table 4, similar parameters were obtained from spectra of the corroded rims of Canyon Diablo and Bear Creek.

After adding the magOx sextet, unexplained features remain at −4 mm s^{-1}, −2 mm s^{-1}, +2 mm s^{-1}, and +4.5 mm s^{-1}, indicative for one or more sextets with B_{hf} significantly smaller than that for any iron oxide or hydroxide. We considered a variety of other phases commonly found in iron meteorites to explain these remaining features, including chalcopyrite, chromite, cohenite, daubreelite, mackinawite, pentlandite, schreibersite, pyrrhotite, and troilite (Lodders and Fegley 1998; Stevens et al. 2002). Based on their Mössbauer parameters (Table 4), chromite and pentlandite can be excluded because their spectra are exclusively composed of doublet phases across the relevant temperature range. Chalcopyrite, daubreelite,

Table 5. Temperature dependent Mössbauer hyperfine parameters for kamacite from Mundrabilla.

T (K)	δ	ΔE_Q (mm s^{-1})	Γ	B_{hf} (T)
195	0.00	0.00	0.47	33.9
205	0.01	0.01	0.49	33.9
215	0.01	0.00	0.46	33.8
225	0.01	0.00	0.47	33.7
235	0.01	0.00	0.46	33.6
245	0.01	0.00	0.46	33.6
255	0.01	0.02	0.45	33.5
265	0.01	0.00	0.45	33.5
275	0.02	0.00	0.46	33.4
285	0.02	0.00	0.44	33.4
295	0.02	0.00	0.43	33.3

Values of δ are given relative to α-iron at the same temperature as the sample. Parameter uncertainties are ±0.02 mm s^{-1} for δ and ΔE_Q and ±0.2 T for B_{hf}.

Table 6. Line widths and line width ratios determined from Meridiani Planum, analog specimens, and a stack of metallic α-iron foils.

Meteorite	Width lines 1 and 6 mm s^{-1}	Width lines 2 and 5 mm s^{-1}	Ratio
Canyon Diablo	0.218	0.166	1.31
	0.221	0.163	1.36
	0.218	0.167	1.31
Bear Creek	0.239	0.186	1.29
	0.236	0.192	1.23
	0.237	0.188	1.26
Mundrabilla	0.244	0.193	1.26
	0.240	0.183	1.31
	0.238	0.183	1.30
North Chile	0.223	0.175	1.27
	0.223	0.177	1.26
Shişr 043	0.225	0.171	1.32
	0.234	0.175	1.34
Iron foil	0.200	0.165	1.21
	0.197	0.161	1.22
Meridiani Planum undisturbed surface	0.275	0.209	1.32
Meridiani Planum brushed surface	0.273	0.204	1.34

Uncertainties for line widths are ±0.02 mm s^{-1}.

mackinawite, pyrrhotite, and troilite do not match the observed features because of their large isomer shifts δ and/or large magnetic hyperfine fields B_{hf}. Cohenite and schreibersite are suitable candidates to explain the observed spectral features. The schreibersite Mössbauer spectrum is composed of three sextets. The cohenite Mössbauer spectrum exhibits a single sextet, which has parameters similar to the intermediate sextet from the schreibersite spectrum. Two separate fits with schreibersite and cohenite, respectively, are shown in Fig. 3. Both phases match the remaining spectral features reasonably well. Because of the low intensity of the peaks in the Mössbauer spectrum of Meridiani Planum, the parameters for both phases were constrained to values obtained from measurements on the Mundrabilla specimen for schreibersite and on the Canyon Diablo specimen for cohenite (Table 4). As we cannot distinguish whether one phase is present while the other phase is absent, we will refer to a combination of both phases ("schreibersite/cohenite") in the remaining text.

With Opportunity's APXS, an enrichment of P, Cl, and S relative to Martian soil was detected in Meridiani Planum (R. Gellert, private communication). APXS spectra obtained on the undisturbed and brushed surface are very similar, suggesting that the enhanced concentrations of P, Cl, and S do not stem from dust on the rock surface. Enrichment in P at least supports indications for the presence of schreibersite. Cl could be present in the nanophase ferric oxide, e.g., in the form of akaganéite. Troilite inclusions may have melted during the descent through the atmosphere (Schröder et al. 2008), or chemically altered after landing (Ashley et al. Forthcoming), leading to the deposition of S on the surface.

With subspectral areas in the range of approximately 5% (Table 3), magOx and schreibersite/cohenite are just above the limit of background counts. However, the spectra obtained on Meridiani Planum are of good statistical quality due to the high iron content of the meteorite. Thus, the peak positions of minor spectral features can be compared between many single temperature windows. The spectra obtained on the undisturbed surface show the smallest subspectral areas of schreibersite/cohenite and magOx (2% schreibersite/cohenite and < 5% magOx compared to 3–4% schreibersite and 7% magOx for any other spectrum). A likely explanation for this is the presence of a small amount of soil and/or dust on the meteorite surface, masking the spectral signatures from schreibersite/cohenite and magOx.

Iron Oxides: Implications for Weathering of Meridiani Planum

Iron oxides, particularly maghemite, but also lepidocrocite, akaganéite, and magnetite, occur as weathering products on iron meteorites found on Earth (White et al. 1967; Bender Koch and Buchwald 1994; Morris et al. 2000). The npOx doublet and the magOx sextet discussed in the Identification of Schreibersite/Cohenite and Iron Oxides in Meridiani Planum section imply the presence of one or more iron oxides as potential weathering phases in Meridiani Planum. These

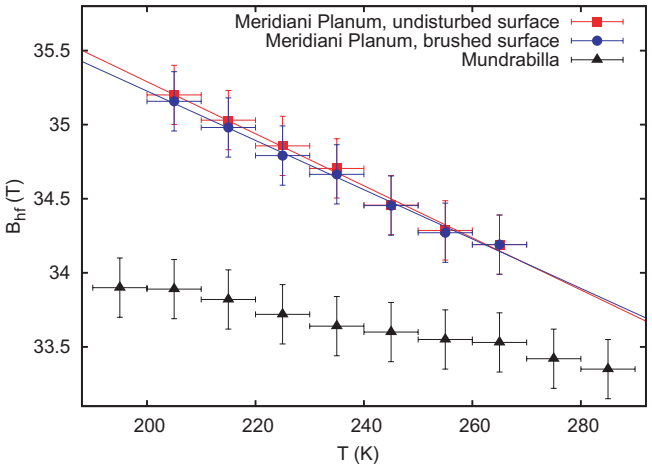

Fig. 5. Temperature dependence of the magnetic hyperfine field B_{hf} of kamacite from Meridiani Planum. Values from spectra obtained on the undisturbed and brushed surface of Meridiani Planum are almost identical. Kamacite from Mundrabilla has smaller B_{hf} values.

oxides are reasonably confined to near surface regions as a discontinuous stain or thin coating and are the origin of the ferric absorption edge observed in Pancam spectra (Schröder et al. 2008). The interpretation of iron oxides as a weathering product related to the discontinuous coating is reinforced based on observations made on two of the three additional iron meteorites encountered by the Opportunity rover. Coated spots on the Block Island and Shelter Island Meridiani meteorites (both measured by IDD instrumentation) were found to contain significantly larger amounts of npOx than uncoated surface portions (Fleischer et al. 2010).

Because both the 14.4 keV and 6.4 keV Mössbauer spectra are dominated by metallic Fe-Ni phases and have the same subspectral areas for the npOx and magOx components, the stain/coating must be thin compared to the penetration depths of both radiations, which are approximately 50 μm as discussed in the Depth Selective Information Extracted from Mössbauer Spectra section. To derive an estimate of the coating's thickness, we simulated Meridiani Planum spectra as described by Fleischer et al. (2008a). As iron oxides and oxyhydroxides are possible candidates for the observed ferric doublet, we assume a chemical composition of 50% np-Fe_2O_3 and 50% np-FeOOH for the ferric doublet. For the phase characterized by the sextet, we assume pure Fe_2O_3. This assumption is one of many possibilities. The thickness would not change significantly assuming a composition of purely np-Fe_2O_3. The simulations suggest an average thickness of less than 1 μm. The coating may be thicker if non-iron–bearing phases are present. It has to be taken into account that the field of view contained coated and uncoated portions of the surface, thus reducing the effect of the surface layer on the spectra. The presence of an oxyhydroxide would strongly suggest interaction with water (including liquid water, frost, or gas–solid interactions) at some time in the surface or near-surface exposure history of the meteorite, and would thus caution against a fusion crust interpretation for the coating. A purely oxidic coating may also have formed through the interaction of the meteorite with atmospheric O_2, but oxidation through the presence of water appears more plausible because the Martian atmosphere is primarily composed of CO_2 (95%) and contains only trace amounts of O_2. Mössbauer spectra obtained on the corroded rims of analog meteorite specimens exhibit spectral features comparable to those observed for Meridiani Planum: a sextet characteristic for iron oxides and a doublet characteristic for (super)paramagnetic iron oxides and/or oxyhydroxides (Table 4). The spectral similarities are another indication that the coatings on Meridiani Planum are a result of chemical weathering rather than a remnant fusion crust. Investigations of the Block Island and Shelter Island coatings, together with additional features not seen in the Meridiani Planum meteorite, are also consistent with a chemical alteration scenario; however, their morphology suggests a higher overall degree of alteration relative to that of the Meridiani Planum meteorite (Ashley et al. Forthcoming). Bland et al. (1998) correlate higher proportion of magnetically ordered ferric oxides with falls during more humid periods in a study of terrestrial age dated ordinary chondritic meteorites from hot desert regions. A direct comparison of the meteorites in this context depends on the timing of their respective fall events in relation to possible aqueous epochs, which is likely to remain unknown.

While the dust layer on Meridiani Planum was thin enough to permit the detection of reflected sky radiance in Mini-TES spectra of Meridiani Planum (which include nonbrushed portions of the rock surface), no obvious signs of the oxide/oxyhydroxide coatings were present in these spectra (e.g., Ashley et al. 2008). Dust deposits within the deeper cavities appear thicker in Pancam images than on other areas of the rock, and weathering products could conceivably be concealed within such protected areas, but this possibility cannot be further explored with the existing data set.

CONCLUSIONS

Mössbauer spectra obtained on the Meridiani Planum meteorite are dominated by kamacite. Mössbauer hyperfine parameters obtained on the undisturbed and brushed surface are identical within the

reported uncertainties over the observed temperature range from 200 K to 270 K. The extrapolation of values for the magnetic hyperfine field B_{hf} to room temperature yields values in good agreement with values obtained from analog measurements and from other studies.

Based on measurements of five analog meteorite specimens, additional minor spectral features can be attributed to the presence of schreibersite and/or cohenite and iron oxides in the meteorite, with subspectral areas of up to 4% and up to 7%, respectively. The contributions of nanophase ferric oxide and magnetically ordered iron oxides (hematite, maghemite and potentially magnetite) to Meridiani Planum spectra are related to the discontinuous surface coating detected in Pancam images.

Simulations of Meridiani Planum spectra suggest a thickness of the coating of less than 1 μm. The presence of iron oxides in a thin coating indicates a low degree of chemical weathering, most likely through the influence of small amounts of water.

Acknowledgments—Development of the MIMOS II Mössbauer spectrometer was funded by the German Space Agency (DLR) under contract 50QM9902 and supported by the Technical University of Darmstadt and the University of Mainz. We thank Dr. Beda Hofmann (Natural History Museum, Bern, Switzerland), and the Senckenberg-Museum (Frankfurt, Germany) for providing meteorite specimens for this study. The support of the Russian space agency is acknowledged. We acknowledge the unwavering support of JPL engineering and MER operations staff and the MER Athena Science Team. We thank A. Kracher and an anonymous reviewer for thoughtful reviews of the manuscript.

Editorial Handling—Dr. Nancy Chabot

REFERENCES

Abdu Y. A. and Ericsson T. 1997. Mössbauer spectroscopy, X-ray diffraction, and electron microprobe analysis of the New Halfa meteorite. *Meteoritics & Planetary Science* 32:373–375.

Al-Kathiri A., Hofmann B. A., Gnos E., Eugster O., Welten K. C., and Krähenbühl U. 2006. Shişr 043 (IIIAB medium octahedrite): The first iron meteorite from the Oman desert. *Meteoritics & Planetary Science* 41:217–230.

Aramu F. and Maxia V. 1970. Shift and broadening of Mössbauer peaks by lack of collimation. *Nuclear Instruments and Methods* 80:35–39.

Ashley J. W., Ruff S. W., Christensen P. R., and Leshin L. A. 2008. Thermal emission spectroscopy of iron meteorites on Earth and Mars—A laboratory evaluation of Meridiani Planum (Heat Shield Rock) (abstract #2382). 39th Lunar and Planetary Science Conference. CD-ROM.

Ashley J. W., Golombek M. P., Christensen P. R., Squyres S. W., McCoy T. J., Schröder C., Fleischer I., Johnson J. R., Herkenhoff K. E., and Parker T. J. Forthcoming. Evidence for mechanical and chemical alteration of iron-nickel meteorites on Mars—Process insights for Meridiani Planum, *Journal of Geophysical Research—Planets*.

Bailey R. E. and Duncan J. F. 1967. Mössbauer and nuclear magnetic resonance studies of several iron phosphides. *Inorganic Chemistry* 6:1444–1447.

Bancroft G. M. 1973. *Mössbauer spectroscopy—An introduction for inorganic chemists and geochemists*. London: McGraw Hill. 251 p.

Bell J. F., Squyres S. W., Herkenhoff K. E., Maki J. N., Arneson H. M., Brown D., Collins S. A., Dingizian A., Elliot S. T., Hagerott E. C., Hayes A. G., Johnson M. J., Johnson J. R., Joseph J., Kinch K., Lemmon M. T., Morris R. V., Scherr L., Schwochert M., Shepard M. K., Smith G. H., Sohl-Dickstein J. N., Sullivan R. J., Sullivan W. T., and Wadsworth M. 2003. Mars Exploration Rover Athena Panoramic Camera (Pancam) investigation. *Journal of Geophysical Research* 108:E12.

Bender Koch C. and Buchwald V. F. 1994. Weathering of iron meteorites from Monuraqui, Chile. *Meteoritics* 29:4.

Bland P. A., Sexton A. S., Jull A. J. T., Bevan A. W. R., Berry F. J., Thornley D. M., Astin T. R., Britt D. T., and Pillinger C. T. 1998. Climate and rock weathering: A study of terrestrial age dated ordinary chondritic meteorites from hot desert regions. *Geochimica et Cosmochimica Acta* 62:3169–3184.

Brückner J., Dreibus G., Gellert R., Squyres S. W., Wänke H., Yen A., and Zipfel J. 2008. Mars Exploration Rovers: Chemical composition by the APXS. In *The Martian surface: Composition, mineralogy, and physical properties*, edited by Bell J. Cambridge, UK: Cambridge University Press. pp. 58–101.

Buchwald V. F. 1975. *Handbook of iron meteorites. Their history, distribution, composition and structure*, vols. 1–3. Center for Meteorite Studies, Arizona State University. Berkeley, CA: University of California Press.

Buchwald V. F. 1977. The mineralogy of iron meteorites. *Philosophical Transactions of the Royal Society of London* 286, No. 1336, 453–491.

Burns R. G. 1993. Mössbauer spectral characterization of iron in planetary surface materials. In *Remote geochemical analysis: Elemental and mineralogical composition*, edited by Pieters C. M. and Englert P. A. J. Cambridge, UK: Cambridge University Press. pp. 539–556.

Christensen P. R., Mehall G. L., Silverman S. H., Anwar S., Cannon G., Gorelick N., Kheen R., Tourville T., Bates D., Ferry S., Fortuna T., Jeffryes J., O'Donnell W., Peralta R., Wolverton T., Blaney D., Denise R., Rademacher J., Morris R. V., and Squyres S. 2003. Miniature Thermal Emission Spectrometer for the Mars Exploration Rovers. *Journal of Geophysical Research* 108:E12.

Connolly H. C., Zipfel J., Grossman J., Folco L., Smith C., Jones R. H., Righter K., Zolensky M., Russell S. S., Benedix G. K., Yamaguchi A., and Cohen B. A. 2006. The Meteoritical Bulletin, No. 90. *Meteoritics & Planetary Science* 41: 1383–1418.

De Grave E., Vandenberghe R. E., De Bakker P. M. A., Van Alboom A., Vochten R., and Van Tassel R. 1992. Temperature dependence of the Mössbauer parameters of

the Fe-Ni phases in the Santa Catharina meteorite. *Hyperfine Interactions* 70:1009–1012.

Dunlap R. A. 1997. A Mössbauer effect investigation of the enstatite chondrite from Abee, Canada. *Hyperfine Interactions* 110:209–215.

Dyar M. D., Agresti D. G., Schaefer M. W., Grant C. A., and Sklute E. C. 2006. Mössbauer spectroscopy of Earth and planetary materials. *Annual Review of Earth and Planetary Sciences* 34, doi:10.1146/annurev.earth.34.031405.125049.

El Goresy A. and Fechtig H. 1967. Fusion crust of iron meteorites and mesosiderites and production of cosmic spherules. *Smithsonian Contributions to Astrophysics* 11:391.

Fleischer I., Klingelhöfer G., Schröder C., Morris R. V., Hahn M., Rodionov D., Gellert R., and de Souza P. A. 2008a. Depth selective Mössbauer spectroscopy: Analysis and simulation of 6.4 keV and 14.4 keV spectra obtained from rocks at Gusev crater, Mars, and layered laboratory samples. *Journal of Geophysical Research* 113:E6.

Fleischer I., Klingelhöfer G., Morris R. V., Schröder C., Rodionov D., and de Souza P. 2008b. Analysis of 6.4 keV Mössbauer spectra obtained with MIMOS II on MER on cobbles at Meridiani Planum, Mars and considerations on penetration depths (abstract #1618). 39th Lunar and Planetary Science Conference. CD-ROM.

Fleischer I., Klingelhöfer G., Schröder C., Mittlefehldt D. W., Morris R. V., Golombek M., and Ashley J. W. 2010, In situ investigation of iron meteorites at Meridiani Planum, Mars (abstract #1791). 41st Lunar and Planetary Science Conference. CD-ROM.

Fultz B. and Morris J. W. 1981. The thickness distortion of ^{57}Fe backscatter Mössbauer spectra. *Nuclear Instruments and Methods* 188:197–201.

Gellert R., Rieder R., Brückner J., Clark B. C., Dreibus G., Klingelhöfer G., Lugmair G., Ming D. W., Wänke H., Yen A., Zipfel J., and Squyres S. W. 2006. Alpha Particle X-ray Spectrometer (APXS): Results from Gusev crater and calibration report. *Journal of Geophysical Research* 108:E12.

Gonser U. 1975. *Mössbauer spectroscopy*. Topics in Applied Physics. vol. 5. Berlin, Heidelberg, New York: Springer. 241 p.

Gorevan S. P., Myrick T., Davis K., Chau J. J., Bartlett P., Mukherjee S., Anderson R., Squyres S. W., Arvidson R. E., Madsen M. B., Bertelsen P., Goetz W., Binau C. S., and Richter L. 2003. Rock abrasion tool: Mars Exploration Rover mission. *Journal of Geophysical Research* 108:E12.

Gütlich P., Link R., Trautwein A., Gütlich P., Link R., and Trautwein A. 1978. *Mössbauer spectroscopy and transition metal chemistry*. Inorganic chemistry concepts, vol. 3. Berlin, Heidelberg, New York/Berlin: Springer. 280 p.

Hawthorne F. C. 1988, Mössbauer spectroscopy. In *Spectroscopic methods in mineralogy*, edited by Hawthorne F. C. Reviews in Mineralogy, 18. Washington, D.C.: Mineralogical Society of America. pp. 255–340.

Herkenhoff K. E., Squyres S. W., Bell J. F., Maki J. N., Arneson H. M., Bertelsen P., Brown D. I., Collins S. A., Dingizian A., Elliott S. T., Goetz W., Hagerott E. C., Hayes A. G., Johnson M. J., Kirk R. L., McLennan S., Morris R. V., Scherr L. M., Schwochert M. A., Shiraishi L. R., Smith G. H., Soderblom L. A., Sohl-Dickstein J. N., and Wadsworth M. V. 2003. Athena microscopic imager investigation. *Journal of Geophysical Research* 108:E12.

Klingelhöfer G., Morris R. V., Bernhardt B., Rodionov D., de Souza P. A., Squyres S. W., Foh J., Kankeleit E., Bonnes U., Gellert R., Schröder C., Linkin S., Evlanov E., Zubkov B., and Prilutski O. 2003. Athena MIMOS II Mössbauer spectrometer investigation. *Journal of Geophysical Research* 108:E12.

Lisher E. J., Wilkinson C., Ericsson T., Häggström L., Lundgren L., and Wäppling R. 1974. Studies of magnetic structure of Fe3P. *Journal of Physics C: Solid State Physics* 7:1344–1352.

Lodders K. and Fegley Jr B. 1998. *Planetary scientist's companion*. New York/Oxford: Oxford University Press. pp. 300–308.

Lovering J. F., Nichiporuk W., Chodos A., and Brown H. 1957. The distribution of gallium, germanium, chromium, and copper in iron and stony-iron meteorites in relation to nickel content and structure. *Geochimica et Cosmochimica Acta* 11:263–278.

Margulies S. and Ehrmann J. R. 1961. Transmission and line broadening of resonance radiation on a resonance absorber. *Nuclear Instruments and Methods* 12:131–137.

Maringer R. E. 1960. Ablation deposits on iron meteorites. *Geochimica et Cosmochimica Acta* 19:5–6.

McCammon C. 1995. Mössbauer spectroscopy of minerals. In *Mineral physics and crystallography: A handbook of physical constants*, edited by Ahrens T. J. AGU Reference Shelf, vol. 2, Washington, D.C.: American Geophysical Union. pp. 332–347.

Mitra S. 1992. *Applied Mössbauer spectroscopy: Theory and practice for geochemists and archaeologists*. Oxford, New York, Seoul, Tokyo: Pergamon Press. 400 p.

Mittlefehldt D. W., McCoy T. J., Goodrich C. A., and Kracher A. 1998. Non-chondritic meteorites from asteroidal bodies, In *Planetary materials*, edited by Papike J. J. Reviews in Mineralogy, vol. 36. Washington, D.C.: Mineralogical Society of America. pp. 195–233.

Morris R. V., Golden D. C., Bell J. F. III., Shelfer T. D., Scheinost A. C., Hinman N. W., Furniss G., Mertzman S. A., Bishop J. L., Ming D. W., Allen C. A., and Britt T. 2000. Mineralogy, composition, and alteration of Mars Pathfinder rocks and soils: Evidence from multispectral, elemental, and magnetic data on terrestrial analogue, SNC meteorite, and Pathfinder samples. *Journal of Geophysical Research* 105:E1.

Morris R. V., Klingelhöfer G., Schröder C., Rodionov D. S., Yen A., Ming D. W., de Souza P. A., Fleischer I., Wdowiak T., Gellert R., Bernhardt B., Evlanov E. N., Zubkov B., Foh J., Bonnes U., Kankeleit E., Gutlich P., Renz F., Squyres S. W., and Arvidson R. E. 2006a. Mossbauer mineralogy of rock, soil, and dust at Gusev crater, Mars: Spirit's journey through weakly altered olivine basalt on the plains and pervasively altered basalt in the Columbia Hills. *Journal of Geophysical Research* 111:E2.

Morris R. V., Klingelhöfer G., Schröder C., Rodionov D. S., Yen A., Ming D. W., de Souza P. A., Wdowiak T., Fleischer I., Gellert R., Bernhardt B., Bonnes U., Cohen B. A., Evlanov E. N., Foh J., Gutlich P., Kankeleit E., McCoy T., Mittlefehldt D. W., Renz F., Schmidt M. E., Zubkov B., Squyres S. W., and Arvidson R. E. 2006b. Mossbauer mineralogy of rock, soil, and dust at Meridiani Planum, Mars: Opportunity's journey across sulfate-rich outcrop, basaltic sand and dust, and hematite lag deposits. *Journal of Geophysical Research* 111:E12.

Morris R. V., Klingelhöfer G., Schröder C., Fleischer I., Ming D. W., Yen A. S., Gellert R., Arvidson R. E., Rodionov D. S., Crumpler L. S., Clark B. C., Cohen B. A., McCoy T. J., Mittlefehldt D. W., Schmidt M. E., de Souza P. A., and Squyres S. W. 2008. Iron mineralogy and aqueous alteration from Husband Hill through Home Plate at Gusev crater, Mars: Results from the Mössbauer instrument on the Spirit Mars Exploration Rover. *Journal of Geophysical Research* 113:E12.

Mössbauer R. L. 2000. The discovery of the Mössbauer effect. *Hyperfine Interactions* 126:1–12.

Murad E. and Cashion J. 2004. *Mössbauer spectroscopy of environmental materials and their industrial utilization*. Boston/Dordrecht/New York/London: Kluwer Academic Publishers. 440 p.

Ortalli I. and Pedrazzi G. 1990. Study of the Torino meteorite. *Hyperfine Interactions* 57:2275–2278.

Ouseph P. J., Groskeutz H. E., and Johnson A. A. 1979. Mossbauer spectra for iron-bearing phases in the meteorite Toluca. *Meteoritics & Planetary Science* 14:97–108.

Rancourt D. G. and Scorzelli R. B. 1995. Low-spin γ-Fe-Ni (γ_{LS}) proposed as a new mineral in Fe-Ni bearing meteorites: Epitaxial intergrowth of γ_{LS} and taenite as a possible equilibrium state at ~20-40 at% Ni. *Journal of Magnetism and Magnetic Materials* 150:30–36.

Rancourt D. G., Lagarec K., Densmore A., Dunlap R. A., Goldstein J. I., Reisener R. J., and Scorzelli R. B. 1999. Experimental proof of the distinct electronic structure of a new meteoritic Fe-Ni alloy phase. *Journal of Magnetism and Magnetic Materials* 191:L255–L260.

Reisener R. J. and Goldstein J. I. 2003. Ordinary chondrite metallography: Part 1. Fe-Ni taenite cooling experiments. *Meteoritics & Planetary Science* 38:1669–1678.

Rieder R., Gellert R., Brückner J., Klingelhöfer G., Dreibus G., Yen A., and Squyres S. W. 2003. The new Athena Alpha Particle X-ray Spectrometer for the Mars Exploration Rovers. *Journal of Geophysical Research* 108:E12.

Riesenman R., Steger J., and Kostiner E. 1969. Cosine effect in Mössbauer spectroscopy involving a source of non-zero radius. *Nuclear Instruments and Methods* 72:109–110.

Schröder C., Rodionov D. S., McCoy T. J., Jolliff B. L., Gellert R., Nittler L. R., Farrand W. H., Johnson J. R., Ruff S. W., Ashley J. W., Mittlefehldt D. W., Herkenhoff K. E., Fleischer I., Haldemann A. F., Klingelhöfer G., Ming D. W., Morris R. V., de Souza P. A., Squyres S. W., Weitz C., Yen A. S., Zipfel J., and Economou T. 2008. Meteorites on Mars observed with the Mars Exploration Rovers. *Journal of Geophysical Research* 113:E6.

Squyres S. W., Arvidson R. E., Baumgartner E. T., Bell J. F. III., Christensen P. R., Gorevan S., Herkenhoff K. E., Klingelhöfer G., Madsen M. B., Morris R. V., Rieder R., and Romero R. A. 2003. Athena Mars rover science investigation. *Journal of Geophysical Research* 108:E12.

Stevens J. G., Khasanov A. M., Miller J. W., Pollak H., and Li Z. 2002. *Mössbauer mineral handbook*. Asheville, NC: Mössbauer Effect Data Center. 750 p.

Van Cromphaut C., Resende V. G., De Grave E., and Vandenberghe R. E. 2007. Mössbauer study of Meridiani Planum, the first iron-nickel meteorite found on the surface of Mars by the MER Opportunity. *Meteoritics & Planetary Science* 42:2119–2123.

Vdovykin G. P. 1973. The Canyon Diablo meteorite. *Space Science Reviews* 14:758–831.

Wasson J. T. and Goldstein J. I. 1968. The north Chilean hexahedrites: Variations in composition and structure. *Geochimica et Cosmochimica Acta* 32:329–339.

Wasson J. T. and Ouyang X. 1990. Compositional range in the Canyon Diablo meteoroid. *Geochimica et Cosmochimica Acta* 54:3175–3183.

Wegener H. 1966. *Der Mössbauer-Effekt und seine Anwendungen in Physik und Chemie*. Mannheim: Bibliographisches Institut Hochschultaschenbücher-Verlag. 226 p.

Weinke H. H. 1977. Chemical and mineralogical investigation of a Mundrabilla specimen. *Meteoritics & Planetary Science* 12:384–386.

White J. S., Henderson E. P., and Mason B. 1967. Secondary minerals produced by weathering of the Wolf Creek meteorite. *American Mineralogist* 52:1190–1197.

Wojnarowska A., Dziel T., Galazka-Friedman J., and Karwowski L. 2008. New mineralogical phases identified by Mössbauer measurements in Morasko meteorite. *Hyperfine Interactions* 186:167–171.